Seventh International Conference on CFD in the Minerals and Process Industries
CSIRO, Melbourne, Australia
9-11 December 2009

TURBULENCE MODEL ANALYSIS OF FLOW INSIDE A HYDROCYCLONE

D.W. STEPHENS* AND K. MOHANARANGAM

Parker Centre (CSIRO Minerals), Clayton, Victoria 3169, AUSTRALIA
*Darrin.Stephens@csiro.au

ABSTRACT

Turbulence analysis of flow inside a hydrocyclone is carried out using commercially available CFD software ANSYS-CFX (release 11.0). Commercial CFD software(s) and their turbulence models have come a long way in accurately predicting the flow inside a hydrocyclone, both at the mean as well as at the turbulence level. Previous studies have shown, the more accurate the turbulence prediction is, the more expensive the simulations are in terms of time. In this paper we have shown, among various turbulence models tested, a two-equation SST (Shear Stress Transport) turbulence model coupled with curvature correction can accurately predict the mean flow behaviour. The same level of accuracy was only found with a SSG Reynolds stress model with a penalty of solving an additional five transport equations. A detailed mesh independency study was carried out to verify the same, in order to minimise any errors from mesh resolution. Experimental data of Monredon et al., (1992) was used to validate our CFD models. SST with curvature correction and SSG turbulence models showed good comparison to both axial as well as tangential velocities along the various sections of the geometry.

NOMENCLATURE

a_1	SST *k-ω* turbulence model constant
a	anisotropy tensor
B	body forces
c_{r1-3}	curvature correction constant
C_{scale}	curvature correction constant
$C_{\varepsilon 1\text{-}2}$	*k-ε* turbulence model constant
C_μ	*k-ε* turbulence model constant
C_{s1-2}	Reynolds stress model constant
C_{r1-5}	Reynolds stress model constant
$C_{\mu RS}$	Reynolds stress model constant
$\sigma_{\varepsilon RS}$	Reynolds stress model constant
D	rate of deformation tensor
F_1	First SST blending function
F_2	Second SST blending function
f_r	streamline curvature strength
$f_{rotation}$	streamline curvature strength
k	turbulence kinetic energy
P_k	shear production of turbulence
P_{kb}	buoyancy production of turbulence
p'	modified pressure
r^*	curvature correction function
$\tilde{r}$	curvature correction function
S	strain rate tensor
t	time
U	velocity
α_3	SST *k-ω* turbulence model constant
β'	SST *k-ω* turbulence model constant
β_3	SST *k-ω* turbulence model constant
ε	turbulence dissipation rate
μ	dynamic viscosity
μ_{eff}	effective viscosity
μ_t	turbulent viscosity
ν_t	kinematic turbulent viscosity
ρ	density
σ_k	*k-ε* turbulence model constant
σ_{k3}	SST *k-ω* turbulence model constant
σ_ε	*k-ε* turbulence model constant
$\sigma_{\omega 2}$	SST *k-ω* turbulence model constant
$\sigma_{\omega 3}$	SST *k-ω* turbulence model constant
Ω	vorticity tensor
ω	turbulence frequency
Φ	pressure-strain correlation
δ_{ij}	kronecker delta

Subscripts

i, j, k	velocity components
mag	magnitude
RS	Reynolds Stress

Superscript

rot	rotation
$(\bar{})$	favre-averaged

INTRODUCTION

Hydrocyclones have found use in numerous industries for over half a century. They are also called the liquid cyclone or the hydraulic cyclone, due to inherent use of water as its primary phase. As they aid in the mechanical separation of dispersed solid particles from a suspension, they have found key applications in the mineral, chemical and pharmaceutical industries, to name a few. In comparison to other mechanical separation devices, hydrocyclones just need energy to overcome the pressure drop they encounter during their operation, making them a cheap alternative (Schuetz et al., 2004). They are also essentially passive devices, with a short residence time making them the ideal device for classification of particles (Brennan, 2006). They work on the principle of

centrifugal forces that develop due to the swirling flow inside the cyclone body that effect particle separation based on their density characteristics. In addition, they are simple in design with low maintenance; this allied with the capacity to handle high throughputs make them the preferred units in many industrial applications.

The very first hydrocyclone models that appeared in the literature were empirical and were capable of predicting the size-classification curve within a reasonable degree of accuracy for a specific flow calibration. While they were good for most flow-sheeting purposes, a CFD model was necessary to study the effect of flow structure with changes in geometry and flow rates. A number of CFD studies were carried out inside a hydrocyclone (Pericleous and Rhodes, 1986; Hsieh and Rajamani, 1991; Dyakowski and Williams, 1993; Malhotra et al., 1994; Rajamani and Devulapalli, 1994). Due to the inherent presence of high swirl and very large curvature of streamlines within the flow, modelling such flow posed a challenge. The high level of turbulence encountered in simulating these flows was not properly represented by the conventional turbulence models (Pericleous and Rhodes, 1986; Malhotra et al., 1994). However, Pericleous and Rhodes (1986) and Hsieh and Rajamani (1991) applied a modified Prandtl mixing-length model for turbulent transport. Their governing equations were formulated in terms of vorticity, stream function and angular velocity, with mixing length being a function of position within the hydrocyclone.

Dyakowski and Williams (1993) proposed a revised approach to modelling turbulent flow in a small diameter hydrocyclone by taking into account the anisotropy of turbulent viscosity, as well as the non-linear interaction between mean vorticity and mean strain rate, by utilising a k-ε model coupled with equations for calculating normal components of Reynolds stresses. Alternatively, Malhotra et al. (1994) tried to capture the turbulence accurately using an altered form of dissipation equation. However, both these works considered that the flow was axi-symmetrical and therefore a two-dimensional equation was solved. The above assumption is not true in the case of industrial hydrocyclones and the error induced in such computations was investigated by He et al. (1999), who concluded that two-dimensional axi-symmetric inlets are far from accurate compared to full three-dimensional ones. The same author also studied the flow pattern inside a hydrocyclone using a modified k-ε model involving a curvature correction term related to the turbulence Richardson number within the dissipation equation.

With increases in computational power, large eddy simulations (LES) are being used as a turbulent closure for resolving the fluid flow inside a hydrocyclone. The advantage is that all of the large eddies are resolved while the small eddies are modelled. The LES approach eliminates the explicit empiricism that is imposed in the k-ε model. Since only the sub-grid scales are modelled in LES, the anisotropy is largely taken care of in this approach (Delgadillo and Rajamani, 2007). Some of the LES studies of hydrocyclones include Brennan (2006), Mainza et al. (2006), Brennan et al. (2007) and Delgadillo and Rajamani (2007, 2009).

In this paper we have shown that in an industrial environment a two-equation model can still be used to depict the turbulence encountered inside a hydrocyclone. It is actually the proper choice of turbulence model and the type of mesh that governs the accuracy of the underlying solution. In this regard, both the unstructured (tetrahedrons) as well as structured (hexahedral) meshes are trialled, along with varying mesh distributions to study the effect of turbulence within these passive devices. In order to verify the validity of the numerical simulations, the results were compared against the experimental data of Monredon et al. (1992).

MODEL DESCRIPTION

A single-phase numerical model was used to simulate the flow in a 75mm diameter hydrocyclone, the dimensions of which are detailed in Monredon et al. (1992). The model is based on the Reynolds Averaged Navier-Stokes equations using the eddy viscosity hypothesis:

Continuity Equation

$$\nabla \bullet (\rho \mathbf{U}) = 0 \tag{1}$$

Momentum Equation

$$\nabla \bullet (\rho \mathbf{U} \otimes \mathbf{U}) = -\nabla p' + \nabla \bullet \left(\mu \left(\nabla \mathbf{U} + \nabla \mathbf{U}^T \right) - \rho \overline{\mathbf{u} \otimes \mathbf{u}} \right) + \mathbf{B} \tag{2}$$

where $\boldsymbol{U}$ is the fluid velocity vector, ρ the fluid density, p' the modified pressure, μ the viscosity, $\rho\overline{\mathbf{u} \otimes \mathbf{u}}$ the Reynolds stresses and $\mathbf{B}$ is the body force.

Two-Equation Turbulence Models

Two-equation turbulence models are widely used in the CFD modelling of many industrial applications; they offer a good compromise between numerical effort and computational accuracy. They derive their name from the fact they solve both the velocity and length scale from two separate transport equations.

The k-ε and k-ω based two-equation models use the gradient hypothesis to relate the Reynolds stresses to the mean velocity gradients and the turbulent viscosity.

$$-\rho \overline{\mathbf{u} \otimes \mathbf{u}} = \mu_t \left(\nabla \mathbf{U} + \nabla \mathbf{U}^T \right) \tag{3}$$

The turbulent viscosity is defined as the product of a turbulent velocity and the turbulent length scale. In two-equation models, the turbulence velocity scale is computed from the turbulence kinetic energy from the solution of a transport equation. The turbulent length scale is estimated from two properties of the turbulence field, usually the turbulence kinetic energy and its dissipation rate. The dissipation rate of the turbulence kinetic energy is provided from the solution of its own transport equation.

k-ε Turbulence Model

Based on the above formulation, the values of turbulence kinetic energy (k) and turbulence dissipation (ε) are obtained by solving differential transport equations and are given by equations (4) and (5), respectively

$$\nabla \bullet (\rho \mathbf{U} k) = \nabla \bullet \left[\left(\mu + \frac{\mu_t}{\sigma_k} \right) \nabla k \right] + P_k - \rho \varepsilon \tag{4}$$

$$\nabla \bullet (\rho \mathbf{U} \varepsilon) = \nabla \bullet \left[\left(\mu + \frac{\mu_t}{\sigma_\varepsilon} \right) \nabla \varepsilon \right] + \frac{\varepsilon}{k} \left(C_{\varepsilon 1} P_k - C_{\varepsilon 2} \rho \varepsilon \right) \tag{5}$$

The turbulent viscosity in equation (3) is computed using the formulation

$$\mu_t = C_\mu \rho \frac{k^2}{\varepsilon} \tag{6}$$

Here C_μ, $C_{\varepsilon 1}$, $C_{\varepsilon 2}$, σ_k and σ_ε are constants. P_k is the turbulence production due to viscous and buoyancy forces, which is modelled using

$$P_k = \mu_t \nabla \mathbf{U} \bullet \left(\nabla \mathbf{U} + \nabla \mathbf{U}^T\right) - \frac{2}{3}\nabla \bullet \mathbf{U}\left(3\mu_t \nabla \bullet \mathbf{U} + \rho k\right) \tag{7}$$

SST (Shear Stress Transport) Turbulence Model

The second set of two-equation turbulence model used in our current study is the *k-ω* based Shear-Stress-Transport (SST) model of Menter (1994). The transport equations for *k* and turbulence frequency (*ω*) are given by equations (8) and (9), respectively

$$\nabla \bullet (\rho \mathbf{U} k) = \nabla \bullet \left[\left(\mu + \frac{\mu_t}{\sigma_{k3}}\right)\nabla k\right] + P_k - \beta' \rho k \omega \tag{8}$$

$$\begin{aligned} \nabla \bullet \left(\rho \mathbf{U} \omega\right) = {} & \nabla \bullet \left[\left(\mu + \frac{\mu_t}{\sigma_{\omega 3}}\right)\nabla \omega\right] \\ & + \left(1 - F_1\right)\rho \frac{2}{\sigma_{\omega 2}\omega}\nabla k \nabla \omega \\ & + \alpha_3 \frac{\omega}{k} P_k - \beta_3 \rho \omega^2 \end{aligned} \tag{9}$$

The combined *k-ε* and *k-ω* models do not account for the transport of the turbulent shear stress, which results in an over-prediction of eddy-viscosity, and ultimately leads to a failed attempt in predicting the onset and the amount of flow separation from smooth surfaces. The proper transport behaviour can be obtained by a limiter to the formulation of the eddy-viscosity and is given by

$$\nu_t = \frac{a_1 k}{\max\left(a_1 \omega, S F_2\right)}; \quad \nu_t = \mu_t / \rho \tag{10}$$

Readers are advised that further information regarding the value of constants and blending functions can be found in the ANSYS-CFX (release 11.0) manual.

SST with Curvature Correction

One of the weaknesses of the eddy-viscosity models is that they are insensitive to streamline curvature and system rotation, which play a significant role in our current hydrocyclone modelling. A modification of the turbulence production term is available to sensitize the standard eddy-viscosity models to these effects. A multiplier is introduced into the production term and is given by $P_k \rightarrow P_k f_r$, where

$$f_r = C_{scale} \max\left\{\min\left(f_{rotation}, 1.25\right), 0.0\right\} \tag{11}$$

The empirical functions suggested by Spalart & Shur (1997) to account for these effects are given by

$$f_{rotation} = \left(1 + c_{r1}\right)\frac{2r*}{1 + r*}\left[1 - c_{r3}\tan^{-1}\left(c_{r2}\tilde{r}\right)\right] - c_{r1} \tag{12}$$

$$r* = \frac{\mathbf{S}}{\mathbf{\Omega}}; \quad \tilde{r} = \Omega_{ij}^{cc}\left(2\Omega_{ik}/\Omega_{mag}\right)/\mathbf{D}^{0.5} \tag{13}$$

$$\Omega_{ij}^{cc} = S_{jk}\left[\frac{DS_{ij}}{Dt} + \left(\varepsilon_{imn}S_{jn} + \varepsilon_{jmn}S_{in}\right)\right]\Omega_m^{rot}/\mathbf{D} \tag{14}$$

$$\Omega_{ij} = 0.5\left[\left(\frac{\partial u_i}{\partial x_j} - \frac{\partial u_j}{\partial x_i}\right)\right] + 2\varepsilon_{mji}\Omega_m^{rot} \tag{15}$$

$$\mathbf{D} = \max\left(\mathbf{S}^2, 0.09\omega^2\right); \quad \mathbf{S}^2 = 2S_{ij}S_{ij} \tag{16}$$

$$\Omega^2 = 2\Omega_{ij}\Omega_{ij}; \quad \Omega_{mag} = \left(\Omega_{12}^2 + \Omega_{13}^2 + \Omega_{23}^2\right)^{0.5} \tag{17}$$

Reynolds Stress Model

Reynolds Stress or Second Moment Closure (SMC) models are applicable where the eddy-viscosity assumption is no longer valid and the results of eddy viscosity models might be inaccurate. They include the solution of transport equations for the individual components of the Reynolds stress tensor and the dissipation rate. The increased number of equations usually leads to reduced numerical robustness, increased computational time and restrictions for usability in complex flows. The standard Reynolds Stress model in ANSYS-CFX is based on the ε-equation. The CFX-Solver solves the following equations for the transport of the Reynolds stresses:

$$\begin{aligned} \frac{\partial}{\partial x_k}\left(U_k \rho \overline{u_i u_j}\right) = {} & \frac{\partial}{\partial x_k}\left(\left(\mu + \frac{2}{3}C_s \rho \frac{k^2}{\varepsilon}\right)\frac{\partial \overline{u_i u_j}}{\partial x_k}\right) + P_{ij} \\ & - \frac{2}{3}\delta_{ij}\rho\varepsilon + \Phi_{ij} \end{aligned} \tag{18}$$

where Φ_{ij} is the pressure-strain correlation and the exact production term P_{ij} is given by

$$P_{ij} = -\rho\overline{u_i u_k}\frac{\partial U_j}{\partial x_k} - \rho\overline{u_j u_k}\frac{\partial U_i}{\partial x_k} \tag{19}$$

The most important term in the Reynolds Stress model is the pressure-strain correlation Φ_{ij} as it acts to drive turbulence towards an isotropic state by redistributing the Reynolds stresses. It can be split into two parts $\Phi_{ij} = \Phi_{ij,1} + \Phi_{ij,2}$, where $\Phi_{ij,1}$ is the 'slow' term, also known as return-to-isotropy term, and $\Phi_{ij,2}$ is called the 'rapid' term. For the SSG model that we used in our current study, these are given by

$$\Phi_{ij,1} = -\rho\varepsilon\left[C_{s1}a_{ij} + C_{s2}\left(a_{ik}a_{kj} - \frac{1}{3}a_{mn}a_{mn}\delta_{ij}\right)\right] \tag{20}$$

$$\begin{aligned} \Phi_{ij,2} = {} & -C_{r1}Pa_{ij} + C_{r2}\rho k S_{ij}\sqrt{a_{mn}a_{mn}} \\ & + C_{r4}\rho k\left(a_{ik}S_{jk} + a_{jk}S_{ik} - \frac{2}{3}a_{kl}S_{kl}\delta_{ij}\right) \\ & + C_{r5}\rho k\left(a_{ik}\Omega_{jk} + a_{jk}\Omega_{ik}\right) \end{aligned} \tag{21}$$

As the turbulence dissipation appears in the individual stress equations, an equation for it is still required and takes the form

$$\begin{aligned} \frac{\partial}{\partial x_k}\left(\rho U_k \varepsilon\right) = {} & \frac{\varepsilon}{k}\left(C_{\varepsilon 1}P - C_{\varepsilon 2}\rho\varepsilon\right) \\ & + \frac{\partial}{\partial x_k}\left[\left(\mu + \frac{\mu_t}{\sigma_{\varepsilon,RS}}\right)\frac{\partial \varepsilon}{\partial x_k}\right] \end{aligned} \tag{22}$$

The constants in the equations take the form $C_{\mu RS}$=0.1, $\sigma_{\varepsilon RS}$=1.36, C_{s1}=1.7, C_{s2}=-1.05, C_{r1}=0.9, C_{r2}=0.8, C_{r3}=0.65, C_{r4}=0.625, C_{r5}=0.2.

NUMERICAL PROCEDURE

The conservation equations of mass, momentum and turbulence given above were solved using a finite volume method in order to determine the single-phase liquid velocity for comparison against the experimental data. It is not possible to arrive at a solution with these equations using analytical approaches; consequently ANSYS-CFX (release 11.0) is used to solve them on structured and unstructured grids. Rhie and Chow (1983) interpolation is used to avoid chequer-board oscillations in the flow field. Coupling between velocity and pressure is handled implicitly by a coupled solver. Advection terms are discretized using the "High Resolution Scheme" which is second-order accurate. In the current study, the air core

was not modelled; rather it was imposed as a free-slip boundary condition along the centre of the hydrocyclone, the width of which was derived from the experiments of Monredon et al. (1992). As a normal CFD practice and a strategy to save computational time, the converged results of the k-ε model was used as an initial guess for the SST model and these results were then used for SST with curvature correction. The converged results from the two-equation turbulence model was not good enough to start the solution process of the SSG model, thereby LRR-IP (a simpler Reynolds Stress model in ANSYS CFX) was run and its results were used as an initial guess for the SSG model. Scalable wall functions within ANSYS CFX were used for k-ε turbulence model, while automatic wall functions were used for SST and its variants and SSG. For the hexahedral meshes the y+ values were typically between 2-400, while for the tetrahedral/prism meshes the values were typically between 7-200.

RESULTS

In this section, the experimental results of Monredon et al. (1992) are compared against our numerical findings. Axial and tangential velocities are compared at three different locations (60mm, 120mm and 180mm from the top of the cyclone). Two different mesh types, pure hexahedral and mixed tetrahedral/prism meshes, where used for the simulations. For each of the mesh types, three different mesh densities were used to assess the effect of mesh resolution on the simulation results. The number of nodes contained in each of the mesh types and densities are shown in Table 1. The results on the finest mesh densities were found to be slightly better than the medium mesh density for both mesh types considered. However, the simulations on the finest mesh density came at an enormous computational cost. Therefore the results using the medium mesh density are presented in this paper. Figure 1 shows the computational mesh for the medium density hexahedral and mixed tetrahedral/prism mesh types.

Table 1: Node number for mesh independency tests

	Coarse	Medium	Fine
Hex	173,000	617,000	1,480,000
Tet/Prism	205,000	728,000	2,800,000

Figure 2 shows the axial and tangential velocities for coarse, medium and fine mesh using hex elements. It could be seen that there is hardly any change from the medium density mesh to the fine mesh. In fact, coarse mesh in our simulations seems to ably replicate the experimental data. However all the results presented in this paper are from medium density meshes.

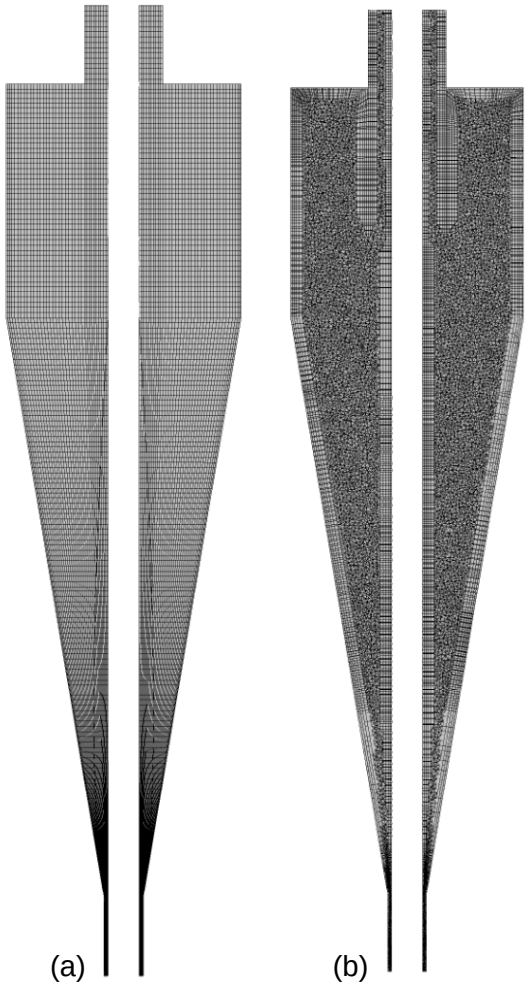

Figure 1: Medium density computational mesh for (a) hexahedral and (b) tetrahedral/prism mesh types.

Figure 3 shows the predicted axial and tangential velocities compared against experimental data using the hexahedral mesh. Here the axial velocities are plotted in the 90^o-270^o plane, whereas the tangential velocities are plotted in the 0^o-180^o plane. The 0^o-180^o plane is normal to the feed port. The left-hand side of the figure shows the axial velocities whereas the right-hand side shows the tangential velocities. Four different turbulence models, namely k-ε, SST, SST with curvature correction (SST-CC) and SSG, are plotted against the experimental data shown in circles.

From the plot of axial velocity at 60mm from the top, it can be seen that the k-ε and SST models fail to capture the flow trend throughout while the SST-CC and SSG models are very good in capturing the vortex flow at the far end and also at the ends of the air core. At 120mm, the same behaviour is observed, however, the SSG model falls short of capturing the magnitude of velocity near the air core, while SST-CC is able to accurately replicate the experimental data. At 180mm, SST-CC is closer to experimental data than SSG, but the asymmetry in the flow structure observed in the experiments is not captured by any of the turbulence models.

Tangential velocities at the 60mm section show a very good comparison for SST-CC and SSG, however, the magnitude of the maximum velocity is not quite replicated

by the SSG model. At the 120mm section the SSG model again fails to compare well with the maximum magnitude while the SST-CC shows a very good match. While SST-CC shows a good match further below at 180mm, the asymmetry between the velocities is still not clearly predicted by the model.

The results presented show neither the k-ε nor SST without curvature correction models perform well. The major reason is the absence of a curvature term which is important for the strong swirling flows in hydrocyclones. This correction appears in the form of a multiplier on the production term in the SST-CC model, whereas in SSG this happens through the pressure-strain correlation which redistributes the Reynolds stresses in the turbulence equations.

Effect of Mesh Types

The long standing issue of whether hexahedral meshes provide better results over tetrahedral/prism meshes is investigated here with the hydrocyclone geometry. It is true that it's rather tedious to obtain pure hexahedral meshes within complex geometries in comparison to tetrahedral/prism meshes.

Figure 4 shows a plot of the axial as well as tangential velocities for three locations from the top (60, 120 and 180mm) for the two mesh types using SST-CC. Axial velocities at location 60mm show a good comparison for both mesh types but as one moves down to the lower conical section of the hydrocyclone the hexahedral mesh outperforms the tetrahedral/prism mesh type. For sections 120 and 180mm the maximum velocity that the tetrahedral/prism mesh predicts is truncated. As mentioned above, the asymmetry in velocities is not well resolved by the models.

For the tangential velocities, sections 60mm and 120mm show a good match for the tetrahedral/prism meshes in comparison to the 180mm section, where the discrepancy is greatest. Throughout various locations the tetrahedral/prism mesh was not able to predict the maximum velocity magnitude observed experimentally.

CONCLUSION

Analysis of different turbulence models was carried out for a turbulent flow inside a 75mm diameter hydrocyclone. Four different turbulence models were tested of which three belong to the two-equation model class and one to the Reynolds Stress class. ANSYS-CFX (release 11.0) was used to solve the governing set of partial differential equations for flow and turbulence. Experimental results of Monredon et al., (1994) were used to compare our numerical findings. For the different turbulence models tested, SST-CC gave the best prediction. The only other model to compete with these predictions is the SSG Reynolds Stress model, with the penalty of solving an additional five equations for varying stresses. Mesh independency tests were carried out to minimise any errors caused due to the underlying mesh. In addition to this, hexahedral and tetrahedral/prism meshes were compared against each other to check the performance of each mesh type in capturing the flow physics within a hydrocyclone. It can be ascertained from this study that hexahedral mesh is still a superior option to tetrahedral/prism mesh in simulating the flow behaviour within a hydrocyclone.

ACKNOWLEDGEMENTS

The authors would like Peter Witt for useful discussions regarding turbulence modelling and boundary conditions in cyclones.

REFERENCES

ANSYS-CFX release 11.0 Reference Manual.

BRENNAN, M.S., (2006). "CFD simulations of hydrocyclones with an air core-comparison between large eddy simulations and a second moment closure", *Trans IChemE (Chemical Engineering Research and Design)*, **84A6**, 495–505.

BRENNAN, M.S., NARASIMHA, M. and HOLTHAM, P.N., (2007). "Multiphase modelling of hydrocyclones-prediction of cut-size", *Minerals Engineering*, **20**, 395-406.

DELGADILLO, J. A. and RAJAMANI, R. K. (2007). "Large-Eddy Simulation (LES) of large hydrocyclones", *Particulate Science and Technology*, **25**, 227-245.

DELGADILLO, J. A. and RAJAMANI, R. K. (2009). "Computational fluid dynamics prediction of the air-core in hydrocyclones", *International Journal of Computational Fluid Dynamics*, **23**, 189-197.

DYAKOWSKI, T. and WILLIAMS, R. A. (1993). "Modelling turbulent flow within a small diameter hydrocyclone", *Chemical Engineering Science*, **28**, 1143-1152.

HE, P., SALCUDEAN, M. and GARTSHORE, I. S. (1999). "A numerical simulation of hydrocyclones", *Trans IChemE (Chemical Engineering Research and Design)*, **77**, 429–441.

HSIEH, K. T. and RAJAMANI, R. K. (1991). "Mathematical model of the hydrocyclone based on physics of fluid flow", *AIChE J*, **37**, 735-746.

MAINZA, A., NARASIMHA, M., POWELL, M. S., HOLTHAM, P. M. and BRENNAN, M. (2006). "Study of flow behaviour in a three-product cyclone using computational fluid dynamics", *Minerals Engineering*, **19**, 1048–1058.

MALHOTRA, A., BRANION, R. M. R. and HAUPTMANN, E. G. (1994). "Modelling the flow in a hydrocyclone", *Canadian Journal of Chemical Engineering*, **72**, 953-960.

MENTER, F.R. (1994). "Two-equation eddy-viscosity turbulence models for engineering applications", *AIAA Journal*, **32**, 1598–1605.

MONREDON, T. C., HSIEH, K. T. and RAJAMANI, R. K. (1992). "Fluid flow model of the hydrocyclones: an investigation of device dimensions", *International Journal of Mineral Processing*, **35**, 65-83.

PERICLEOUS, K. A. and RHODES, N. (1986). "The hydrocyclone classier—A numerical approach", *International Journal of Mineral Processing*, **17**, 23-43.

RAJAMANI, R. K. and DEVULAPALLI, B. (1994). "Hydro dynamic modeling of swirling flow and particle classification in large-scale hydrocyclones", *KONA-Powder and Particle*, **12**, 95-104.

RHIE, C.M. and CHOW, W.L. (1983). "Numerical study of the turbulent flow past an airfoil with trailing edge separation", *AIAA Journal*, **21**, 1527-1532.

SCHUETZ, S., MAYER, G., BIERDEL, M. and PIESCHE, M. (2004). "Investigations on the flow and separation behaviour of hydrocyclones using computational fluid dynamics", *International Journal of Mineral Processing*, **73**, 229-237.

SPALART, P.R. and SHUR, M. (1997). "On the sensitization of turbulence models to rotation and curvature", *Aerospace Science and Technology,* **1**(5), 297-302.

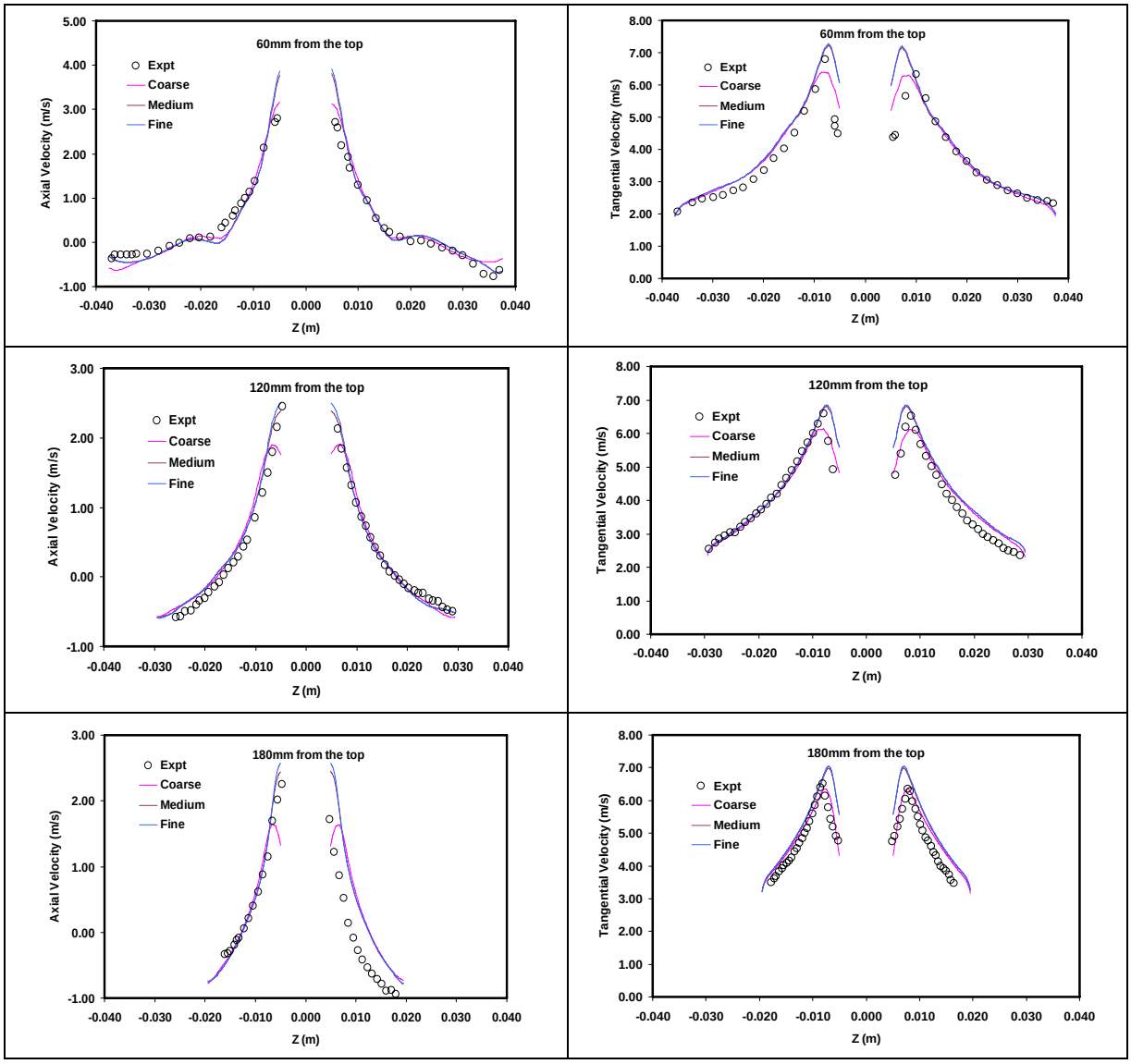

Figure 2: Axial and Tangential velocities at various vertical locations in the hydrocyclone for varying node numbers of hexahedral elements using SST with curvature correction

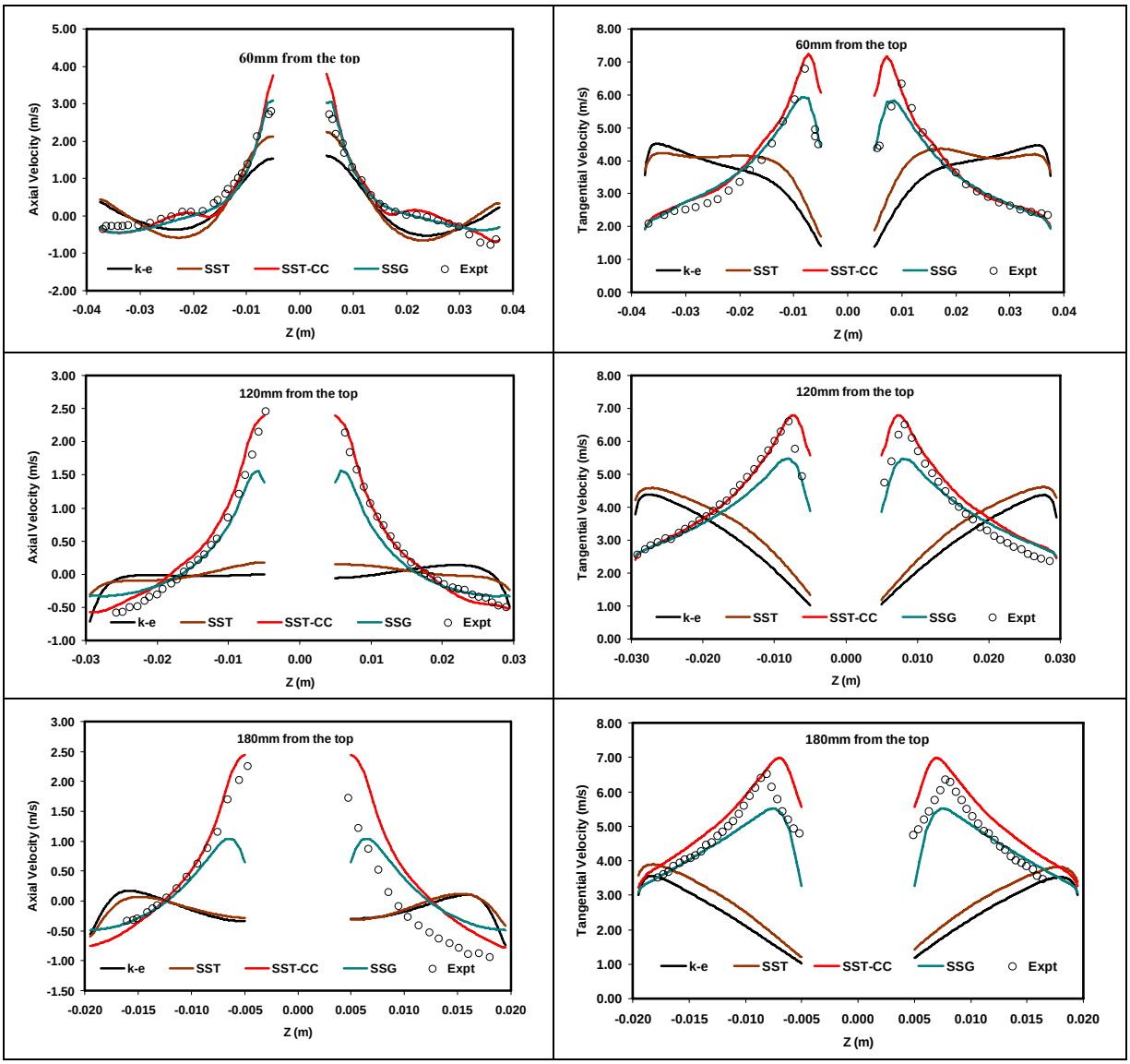

Figure 3: Comparison of Axial and Tangential velocities at various vertical locations in the hydrocyclone for the four turbulence models tested on the medium density hexahedral mesh.

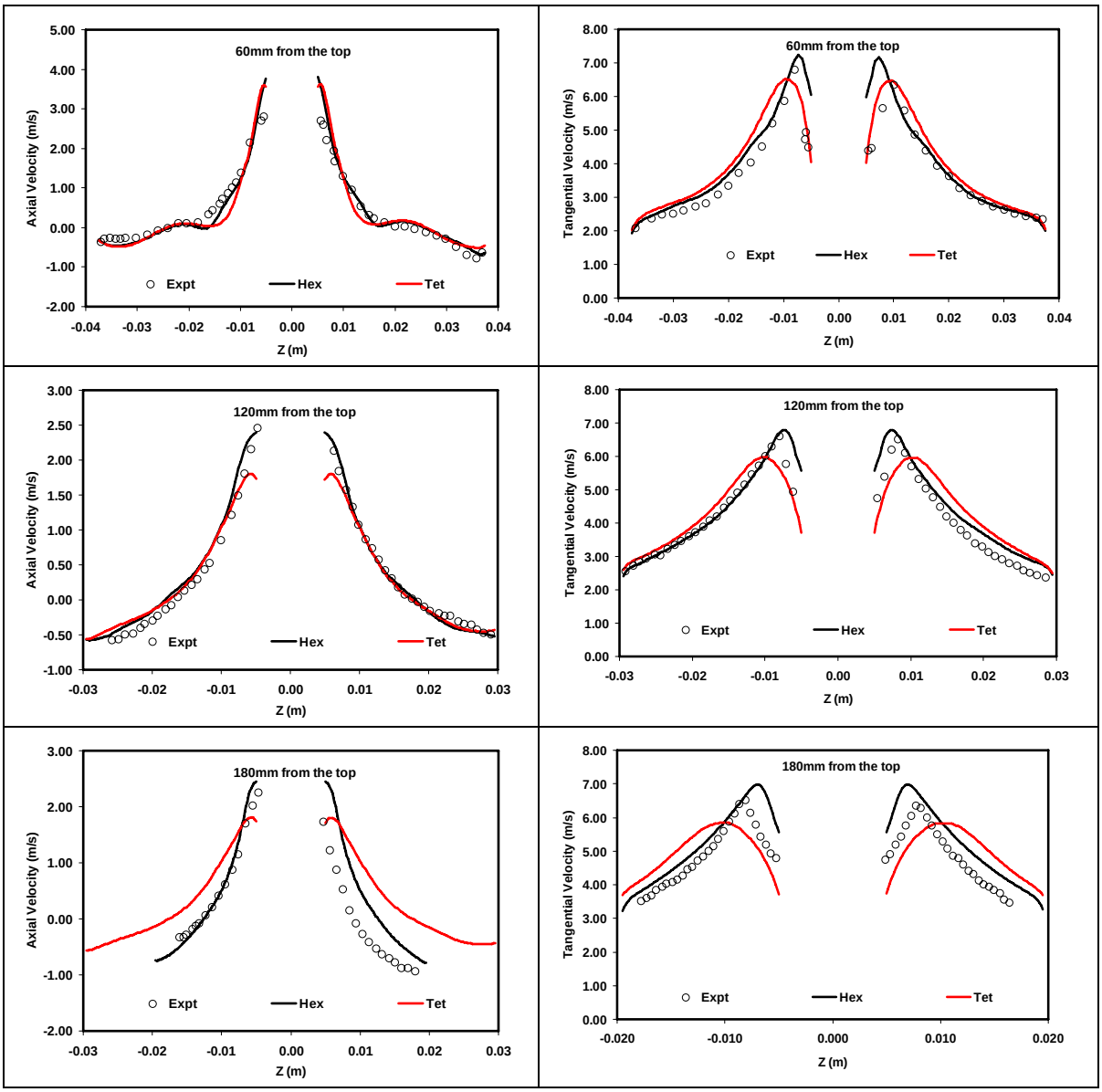

Figure 4: Comparison of Axial and Tangential velocities with hexahedral and tetrahedral/prism meshes for the SST-CC turbulence model using the medium density meshes.